Steady-State Free Precession sequences for high and low field NMR spectroscopy in solution: Challenges and opportunities

Tiago Bueno Moraes [a,*], Flávio Vinícius Crizóstomo Kock [b], Kahlil Schwanka Salome [c], Andersson Barison [c], Andre Simpson [b], Luiz Alberto Colnago [d,*]

[a] *Universidade de São Paulo/ESALQ, Depto. Engenharia de Biossistemas, Av. Páduas Dias, 11, Piracicaba, SP, 13418-900, Brazil*
[b] *Department of Physical and Environmental Sciences, University of Toronto Scarborough Campus, 1265 Military Trail, Toronto, ON, M1C 1A4, Canada*
[c] *NMR Lab., Department of Chemistry, Federal University of Paraná, Curitiba, PR, 81530-900, Brazil*
[d] *Embrapa Instrumentação, Rua XV de Novembro 1452, São Carlos, SP, 13560-970, Brazil*

ARTICLE INFO

ABSTRACT

The receptivity of NMR spectroscopy is low when compared to other techniques. Historically, increasing the strength of the static magnetic field has been the major approach to increase NMR sensitivity. In recent years several polarization transfer protocols have been used to enhance the signal-to-noise ratio (SNR), although they require special accessories and/or sample preparation. In this paper, we consider both the challenges and opportunities of steady-state free precession (SSFP) pulse sequences as a simple and efficient alternative to enhance SNR, in standard high-resolution and benchtop low-resolution NMR spectrometers. The maximum gain in these sequences is obtained with the shortest time between the pulses (Tp). However, when $Tp<T_2$, the SSFP signal contains FID and echo components which lead to phase, intensity, and truncation artifacts on spectra obtained by Fast Fourier transform (FT). Several phase alternation SSFP sequences were used to cancel the echo component and minimize these problems in the FT spectra. Krylov base diagonalization method (KBDM) was used to eliminate the phase and truncation problems in spectra acquired by SSFP pulse sequences and can be a viable alternative to FT. The experiments were performed in high and low resolution (bench top) NMR spectrometers and significant enhancements in SNR of low receptivity nuclei such as ^{13}C and ^{15}N could be achieved. The SSFP sequences were also shown to enhance SNR in nuclei with high receptivity such as ^{19}F and ^{31}P, in very dilute samples, as is common in environmental and biological samples.

Introduction

The NMR signal-to-noise ratio (SNR) is very low when compared to other higher frequency spectroscopies (i.e. microwave, infrared, visible, etc.). This low SNR is due to the very small difference between the populations of nuclear spin energy levels, which are only observed in presence of a magnetic field (Zeeman effect) [1]. The spin population in each energy level is dependent on the magnetic field strength (B_0) and the intensity of NMR signals increases with $B_0^{3/2}$. The NMR spectral resolution (i.e. the signal separation) also depends on B_0 as the chemical shift increases linearly with it and the spectral line width depends on the B_0 inhomogeneity (ΔB_0), in the sample volume. Therefore, the development of magnets with very high B_0, with minimal ΔB_0, is a constant challenge for NMR spectroscopy. Magnets with the highest B_0 and with minimal ΔB_0 are normally obtained with superconducting magnets [2].

The coils have to be maintained at very low temperature (i.e. in liquid helium) and therefore they are very expensive and the highest field magnets available (for example 1.2 GHz) have a prohibitive purchase value for most laboratories, associated with the maintaining costs makes them inaccessible for most academic and industrial labs [3].

Therefore, compact or benchtop NMR spectrometers, based on low field permanent magnets ($B_0 < 3T$) with minimal maintenance costs have emerged over the last decade [3,4]. These new instruments are rapidly gaining importance in academia and industry as they are low-cost, cryogenic-free systems, able to obtain spectra with enough resolution for a broad range of applications including structural determination, quantitative analysis, quality control, reaction, flow, and process monitoring among others. However, one of the limitations of benchtop instruments, in comparison to high field systems, is the much lower signal-to-noise ratio (SNR).

Therefore, several approaches have been proposed to enhance SNR in NMR, not only for low-field but also for high-field instruments, especially for nuclei with low receptivity (i.e. low natural abundance and/or low gyromagnetic constant) and long longitudinal relaxation time (T_1), such as ^{13}C or ^{15}N [5]. Limits of detection (LOD) or limit of quantification (LOQ) can also be an issue for high-field instruments using even high receptivity nuclei such as ^{1}H, ^{19}F, and ^{31}P, for very diluted samples, normally found in natural product extractions, environmental samples, and biological fluids [6–9].

The most common way to increase SNR, and consequently lower the LOD and LOQ in the NMR is to average many (n) Free Induction Decays (FID) signals. However, enhancement in SNR is proportional to $\sqrt{n}$ (where n= number of scans), and a two-fold increase in SNR requires four times the measurement time. Other more sophisticated technologies have been used to enhance SNR in low or high field NMR spectroscopy. They are based on polarization transfer protocols such as dynamic nuclear polarization (DNP), optical pumping, parahydrogen-induced polarization, indirect detection in 2D experiments etc [5,10,11]. However, in almost all these methods it is necessary to use special accessories, special sample preparation, even both. Also, some of the approaches are selective in their enhancements (i.e. not all nuclei are observed), while in other cases, the need to add radicals can reduce spectral resolution and produce artifacts.

On the other hand, a solution that has been widely used to enhance SNR (or permit faster acquisition) in magnetic resonance imaging (MRI) [12,13] and time domain NMR (TD-NMR) relaxometry is the use of the Steady State Free Precession pulse sequences (SSFP) [14,15]. However, these sequences are rarely used in solution-state NMR spectroscopy [16] and were only recently applied in solid-state NMR [17]. Therefore, challenges and opportunities of SSFP sequences to enhance SNR (or for fast NMR measurements), in solution, will be presented.

Steady state free precession pulse sequences

Bradford et al. (1951) observed a continuous NMR steady state signal when a sample was excited with equally spaced pulses with a repetition time (T_p) equal to or shorter than the transverse relaxation time T_2 [18]. H.Y. Carr in 1958 [19], also demonstrated that when a spin system is subject to a series of radiofrequency pulses, with the same phase, flip angle, and $T_p < T_1, T_2$ it reaches a special steady-state regime, which he named Steady State Free Precession (SSFP). The spin system reaches the SSFP regime, independent of the initial condition, with an exponential time constant T*, that depends on T_1 and T_2 and the flip angle θ according to Eq. 1,[20–22].

$$T^* = \frac{2T_1T_2}{T_1(1-\cos\theta)+T_2(1+\cos\theta)} \tag{1}$$

The amplitude of the magnetization in the SSFP regime (*Mss*) is described by Eq. 2, it is a function of the flip and precession angles and relaxation times [20–27].

$$\frac{Mss}{M_0} = \frac{|\sin\theta|\sqrt{2-2\cos\Phi}}{(1+\cos\theta)(1-\cos\theta)+2(1-\cos\theta)T_1/T_2} \tag{2}$$

where, $\Phi = \Omega T_p$ is the precession angle and Ω is the frequency offset, T_p is the time between pulses, M_0 is the magnetization at thermal equilibrium, and T_1 and T_2 are the relaxation times. The solutions to these equations can be found elsewhere [28].

When $T_p \leq T_2$ the SSFP signal is composed of an FID signal after each pulse and by a *reversed-FID* signal (echo component), that is formed by spin echoes and stimulated echoes of all the previous pulses [17,22,24]. Fig. 1 shows the SSFP signal for acquisitions times (Aq) $T_2^*<Aq<T_2$, composed by an FID and echo components without strong overlap. The SSFP signal in this figure uses an acquisition time (Aq)~T_p and a recycle delay, D1<<Aq [26]. T_2^* is the effective transverse relaxation time that depends on T_2 and ΔB_0.

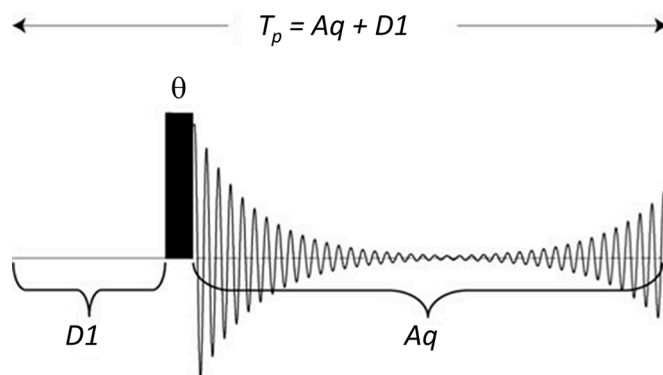**Fig. 1.** SSFP signal showing the FID and echo components for $T_2^*<Aq<T_2$, where T_p is the pulse interval, Aq is the acquisition time and D1 is the recycle delay (D1<<Aq). Normally, D1 is the minimum recycle delay allowed by the NMR instruments.

When $T_p < T_2^* < T_2$ the FID and echo overlap, allowing constructive or destructive interactions that yield signals with maximum and minimum amplitude, respectively [19]. Under very short pulse intervals (T_p=0.3 ms) thousands of SSFP signals can be summed per second [15] making the SSFP one of the best NMR pulse sequences to provide spectra with the highest SNR/time ratio [17]. The special SSFP regime ($T_p < T_2^*$) is known as Continuous Wave Free Precession (CWFP) because the magnitude of the NMR signal does not decay to zero if the pulse excitations are maintained.

The CWFP pulse sequences with very short T_p have been widely used in time domain NMR (TD-NMR), where spectral resolution is not required. They have been used to enhance SNR [15,29], to measure liquid flow [14], in quantitative online measurements [30], fast polymerization reactions [31], and fast thermal diffusion measurements [32]. The CWFP sequences have also been used to measure T_1 and T_2 in a fast and single experiment [31]. It also can be used to obtain the full T_1 curve in a single shot experiment [20], that have been used as the direct dimension in 2D T_1-T_2 and T_1-D experiments [25,33,34]. Furthermore, CWFP sequences have been used in high resolution NMR, as a method to suppress strong solvent signals before the signal acquisition [35]. However, these CWFP sequences have not been used in imaging (MRI) and NMR spectroscopy because they do not have spatial or frequency resolution. Therefore, the applications in MRI or NMR spectroscopy must be performed using conventional SSFP sequences, without strong overlap of the FID/echo components.

Rapid spectral acquisition using phase alternation SSFP sequences

When Ernst and Anderson introduced the pulsed and Fourier transform NMR spectroscopy in 1966, they derived the Bloch equations to calculate the pulsed NMR signals, including the signals in the SSFP regime [23]. They demonstrated that the amplitude of FID and echo signals, in the SSFP regime, can be calculated as a function of T_p, T_1, T_2, θ and Φ angles. They demonstrated that the NMR signal must be acquired with $T_p>3T_2$, to have minimal echo intensity and consequently minimal spectral anomalies. They also demonstrated that for maximum SNR enhancement is necessary to optimize T_p and θ, which provides an SNR increase with the reduction of T_p.

In 1971 Freeman and Hill [36] and Schwenk [27] proposed procedures to minimize the phase and amplitude anomalies in high-resolution NMR spectra obtained in the SSFP regime ($T_p \leq T_2$). These anomalies are due to the echo component in SSFP signals. Freeman/Hill method, named Scrambled Steady-State was based on a variation of the T_p, that suppress the echo component due to oscillation in the echoes phase. This procedure is efficient only when the signals are far from the resonance frequency, as normally used in early NMR receivers, without quadrature detection. With quadrature detection, the

echo signals at or close to resonance frequency cannot be suppressed with this procedure [37]. The Schwenk procedure was based on the use of four-resonance frequency and was named Quadriga Fourier transform. To the best of our knowledge, these SSFP procedures were never implemented in high-resolution routine NMR analysis.

More recently we have proposed the use of magnitude spectra and the use of Traf (Trafficante's [38]) apodization function to remove phase and truncation anomalies in ^{13}C spectra [37]. We also used parametric methods like Filter Digitalization Method (FDM) or Krylov Base Diagonalization Method (KBDM) to obtain SSFP spectra without the phase and truncation anomalies, observed in spectra obtained using Fourier transform (fast Fourier transform algorithm) [16,39]. However, no post-acquisition processing method can solve the amplitude problem because the intensity of the peak signals in SSFP spectra can be reduced or suppressed by the destructive interference between FID and echo signals. Therefore, this effect of peak amplitude suppression must be eliminated during the time domain NMR signal acquisition.

In magnetic resonance imaging (MRI) the amplitude anomaly has been minimized by the acquisition of SSFP pulse sequences with and without pulse phase alternations that suppress the echo component. These procedures have been successfully implemented in MRI to eliminate banding artifacts caused by the echo component [12,13]. These SSFP methods have achieved high efficiency, in terms of SNR and reducing measuring time [40] in functional FMRI [41]. Rudakov et al. [42,43] also used SSFP sequences with phase alternation of the pulses to improve the SNR in ^{14}N Nuclear Quadrupole Resonance (NQR). Recently the Frydman group used the SSFP sequences with phase alternation to enhance SNR in solid-state NMR of quadrupolar nuclei [17].

These procedures, used in NQR, MRI, or solid-state NMR, reduce the effect of the echo component in SSFP signals and requires the acquisition of at least two experiments. One SSFP sequence uses a train of pulses with constant phase and another SSFP sequence with the phase of the pulses alternated by π. The addition of these two signals gives an SSFP signal with minimal echo component and consequently minimal amplitude anomalies.

In the last decade, the Colnago group started to use similar phase alternation protocols to mitigate phase and amplitude anomalies in high-resolution solution NMR [22]. In this work, we demonstrated the uses of *constant phase increment* SSFPdx and *non-constant phase increment* SSFPdxdt to minimize amplitude, phase, and truncation anomalies in SSFP spectra, and provide a rapid acquisition or high SNR, not only for benchtop NMR, but also for high-resolution spectrometers.

SSFP pulse sequences with phase increment: SSFPdx and SSFPdxdt

Eq. 2 shows the dependence of the amplitude of the magnetization (M_{ss}) in the SSFP regime for conventional SSFP sequence, composed of equidistant pulses, and constant phase, as a function of θ, Φ, T_p and the relaxation times T_1 and T_2.

For time intervals $T_2^* < T_p << T_1, T_2$, the FID and echo overlap in the SSFP sequence with constant phase (Fig. 2A). This figure shows a 180° phase difference between FID and echo components. The overlap between FID/echo components results in an excitation profile in the frequency domain, with constructive or destructive interferences, with null signals in multiple positions ($\Phi = 2n\pi$) and maximum signals for $\Phi = (2n+1)\pi$ (Fig. 2B). The periodic null amplitudes occur at $1/T_p$ Hz, as shown in Fig. 2B. Using $T_p = 0.1$ s the null points are spaced by 10 Hz in the frequency domain.

Fig. 2C shows the SSFP signal obtained by the SSFP sequence with
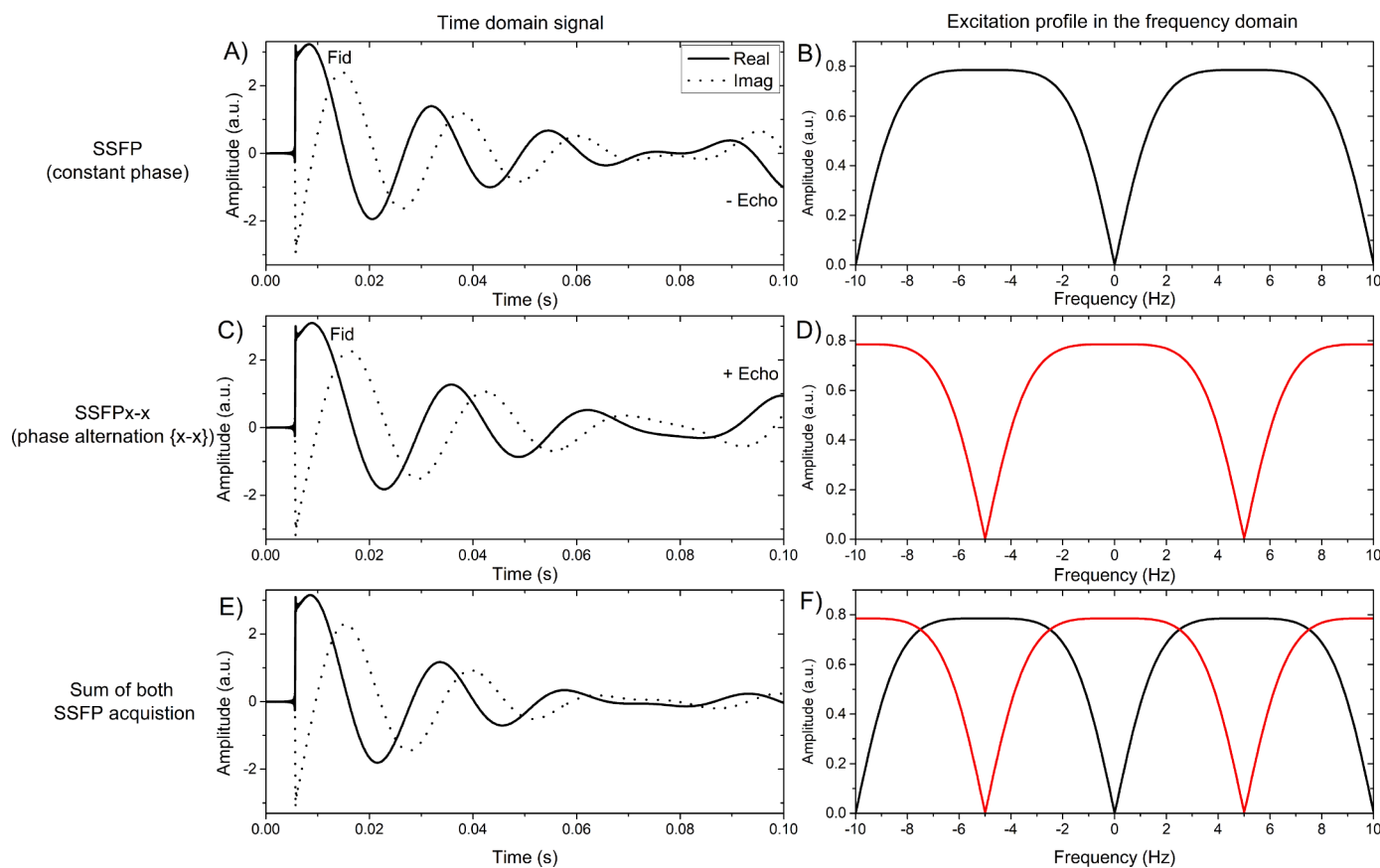
Fig. 2. SSFP signals acquired using $T_p = 0.1$ s, for a sample of 20 µl of H_2O in 500 µl of D_2O. The left column shows the signal obtained with SSFP with constant phase (A), the signal acquired with SSFP with phase alternation of π and the sum of signals A and C (E) that suppress the echo component. The right column shows the excitation profiles of the SSFP sequences B, D, and F for the respective experiments in the left column.

the pulses and receiver phases alternating by π. The SSFP signal with phase alternation also shows an overlap between FID/echo components. However, the FID and echo signals have the same phase. The SSFP excitation profiles for pulses with phase alternation of π (Fig. 2D) show the maximum amplitude for $\Phi = 2n\pi$ and minimum amplitude for $\Phi = (2n + 1)\pi$. The periodic null amplitudes, in the frequency domain, also occur at $1/T_p$ Hz. However, the nulls are in the maximum amplitude of the signals obtained with the SSFP sequence with constant phase.

When the SSFP signals of the two experiments (Fig. 2A and 2C) are summed, the echo component is suppressed, because of the phase difference of 180° in the echoes signals, resulting in an SSFP signal with only the FID component (Fig. 2E). This figure also shows that the last data points of the signals are closer to zero than the last data points of signals A and C. This data points closer to zero in Fig. 2E also results in the minimization of the truncation problem from the Fourier transformed spectrum.

This suppression can also be seen by adding the two excitation profiles of Figs. 2B and 2D, resulting in an excitation profile without null amplitudes (Fig. 2F). However, the sum of only two experiments with and without phase alternation, the excitation profile still shows some amplitude modulation [12].

The reduction of this amplitude modulation along the frequency offset can be done by reducing the phase angle increment in the SSFP sequences. When a constant increment, $\Delta\varphi$, is applied from excitation to excitation $\varphi(n) = \varphi_0 + (n - 1)\Delta\varphi$, and the receiver phase following the same scheme, the excitation profile is shifted by

$$\Delta f = \frac{\Delta\varphi}{2\pi T_p} \qquad (2)$$

along the frequency axis.

Fig. 3 shows the simulated (A to D) and experimental (E to H) excitation profiles for a water sample using SSFP with and without phase increments. Figs. 3A and 3E show the SSFP profiles without phase

increment with typical maximum and minimum values. Fig. 3B shows the profile of the SSFP signals (SSFPd2) without and with π phase increment. The experimental profile using only two SSFP sequences (Fig. 3F) shows a small amplitude modulation, that is also observed in MRI experiments in similar conditions [12]. Figs. 3C and 3G and 3D and 3H, show the excitation profiles for 4 (SSFPd4) and 8 (SSFPd8) experiments with {0, $\pi/2$, π and $3\pi/2$} and {0, $\pi/4$, $\pi/2$, $3\pi/4$, π, $5\pi/4$, $3\pi/2$ and $7\pi/4$} phase increments, respectively. The sum of these signals with 4 or 8 phase increments shows a uniform excitation profile for a wide range of frequency offsets, without any amplitude modulation. This is equivalent to the elimination of the destructive or constructive interaction between FID and echo signals. Smaller phase increments can also be used to improve the excitation profile.

Another way to suppress the echo component and eliminate the null amplitude in the SSFP profile is to use sequences with *non-constant phase increment*, called SSFPdxdt [22]. In these sequences, the phases are incremented by

$$\varphi(n) = \varphi_0 + A(n - 1)^2 \qquad (3)$$

where n corresponds to an integer number (n = 1,2,3, ...) that represents each applied pulse of the sequence and A is a constant value and defines how fast the phases are incremented quadratically. Quadratic phase increments using A = $\pi/512$, $\pi/256$, $\pi/128$, $\pi/64$, $\pi/32$, $\pi/16$, $\pi/8$, and $\pi/4$ and $\pi/2$ have been implemented and the resulting phase table for TopSpin Bruker are showed in the Supplementary Material. Figure S1 shows that using A from $\pi/2$ to $\pi/64$ results in low amplitude at the excitation profile and best SSFP amplitude are obtained using A = $\pi/256$ and $\pi/512$. These pulse sequences show similar results to SSFPdx sequences in the samples studied, with the advantage that it can be performed in one block acquisition. Scripts for all SSFP pulse sequences developed for Bruker's TopSpin can be found at the Supplementary Material.

The SSFP excitation profiles and signal amplitude also depend on flip
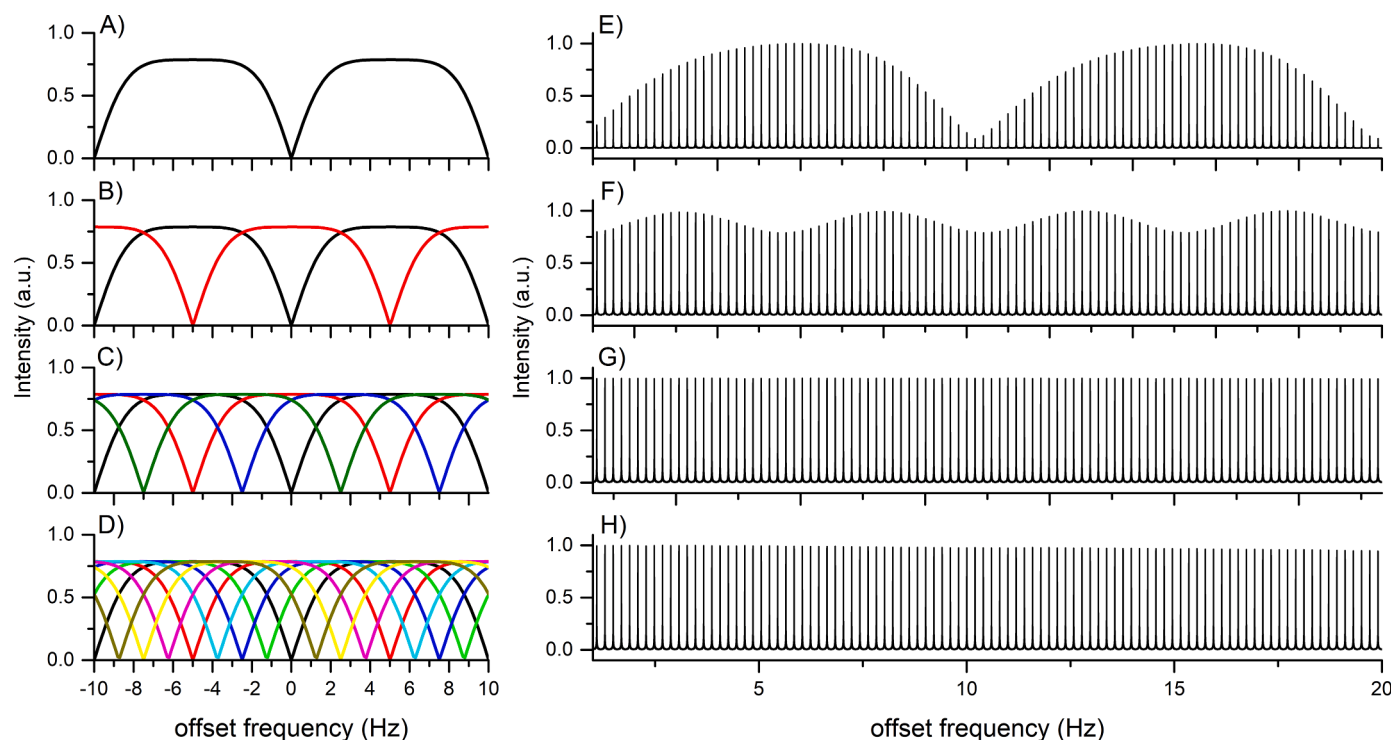
Fig. 3. Simulated and experimental excitation profile of conventional SSFP pulse sequence with and without phase alternation for water signal at several frequency offsets for a sample composed of 20 µl of H_2O in 500 µl of D_2O. A) without phase increment. B) with {0 and π} phase increment (SSFPd2), C) {0, $\pi/2$, π and $3\pi/2$} (SSFPd4) and D) {0, $\pi/4$, $\pi/2$, $3\pi/4$, π, $5\pi/4$, $3\pi/2$ and $7\pi/4$} (SSFPd8) phase increments. The null regions of the excitation profile are canceled using multiple acquisition SSFP blocks, for instance, SSFPd2, SSFPd4, and SSFPd8.

angle θ and T_1/T_2 ratio as described by Eq. (2). Fig. 4 resumes the behavior of Eq. (2), in function of flip and precession angles (Φ) and in function of T_1/T_2 ratio.

Materials and methods

D$_2$O (99.9% D), ACN-d_3(99.9% D), DMSO-d_6 (99.8% D, brucine, glucose, sucrose, aniline, and triethylamine were purchased from Sigma-Aldrich and used as it. The concentration of each sample is described in the figure captions.

High-resolution SSFP experiments at 14.1 T

The high-resolution NMR experiments were performed on a high-field Bruker AVANCE III 600 spectrometer, operating at 14.1 T, observing ^{1}H, ^{13}C, and ^{15}N at 600, 150, and 60 MHz, respectively. Conventional ^{13}C{^{1}H} spectra were acquired using standard pulse *zgpg30* sequences from the Bruker library, with Aq= 0.9 s and recycle delay (D1) of 2 s. The conventional ^{15}N experiments were performed with the default zg pulse sequence with Aq= 2 s and D1= 2s.

The pulses and phase alternations of SSFPdx sequences for TopSpin (Bruker) are performed sequentially (supplementary material 1). The SSFPdx signals are obtained sequentially, starting with the sequence without phase alternation (SSFP) (left) followed by an SSFP sequence with phase alternation by π, SSFPx-x (right). Fig. 5 illustrates the simulated signals obtained SSFPd2 pulse sequence for two peaks. The SSFP signals at the top and bottom were simulated for a sample with two signals. The left side of the top signal shows the minimum signal, for the peak at resonance (SSFP) and a maximum signal for the SSFPx-x sequences. The left side of the bottom signal shows the maximum signal, for the peak at resonance (SSFP) and a minimum signal for the SSFPx-x sequences. The signal obtained by the SSFPd2 sequence is the sum of SSFP and SSFPx-x signals, Fig. 5.

In the sequences programmed using TopSpin, the dummy scans (DS) and the number of scans (NS) parameters are not used and must be set to 1 and were replaced by L_0 and L_1, respectively.

The sequence starts executing L_0 dummy scans, to reach the steady-state of the first phase increment, then execute L_1 scans to acquire the SSFP signals. Subsequently, the sequence starts executing L_0 dummy
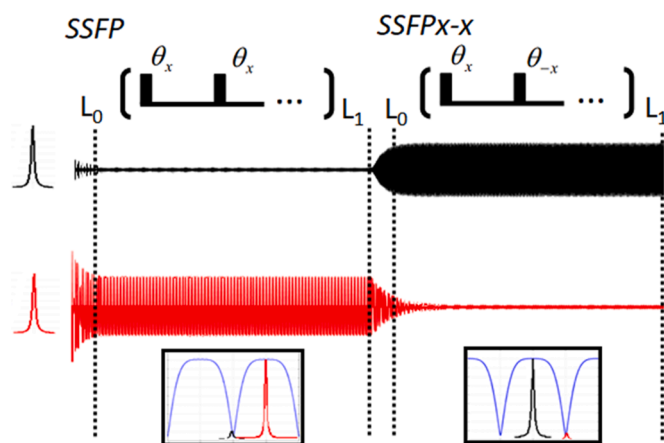

Fig. 5. Illustration of sequentially SSFP acquisitions for the programmed SSFPd2 pulse sequence (SSFP and SSFPx-x components), where L_0 is the dummy of scans and L_1 is the number of scans of each block.

scans and L_1 scans to acquire the SSFPx-x signals. SSFPd4 and SSFPd8 pulses sequence are based on the same protocol by adding 4 or 8 SSFP signals, sequentially.

The SSFP sequences without phase increment were simply the default zgpg30 pulse sequences with short Tp values and D1 = 0.01s. The SSFP sequences with multiple block acquisition using constant phase increment composed by the sum of SSFP signals with phase increment composed by 2 (SSFPd2), 4 (SSFPd4), and 8 (SSFPd8) blocks: i) SSFPd2 is the sum of SSFP experiments with 0 and π phase increments; ii) SSFPd4 is the sum of SSFP experiments with 0, $\pi/2$, π and $3\pi/2$ phase increments, and iii) SSFPd8 is the 0, $\pi/4$, $\pi/2$, $3\pi/4$, π, $5\pi/4$, $3\pi/2$ and $7\pi/4$ phase increments. We also used SSFP sequences with a quadratic phase increment (SSFPdxdt), that was implemented using A = $\pi/256$ and A = $\pi/512$, Eq. (3).

All ^{13}C SSFP spectra were proton decoupled with the power-gated decoupling (waltz-16). The D1 with and without decoupling were 10 and 0.1ms, respectively. The ^{1}H and ^{15}N SSFP acquisition mimic the ^{13}C parameters described. The number of scans (NS) and flip angle θ are

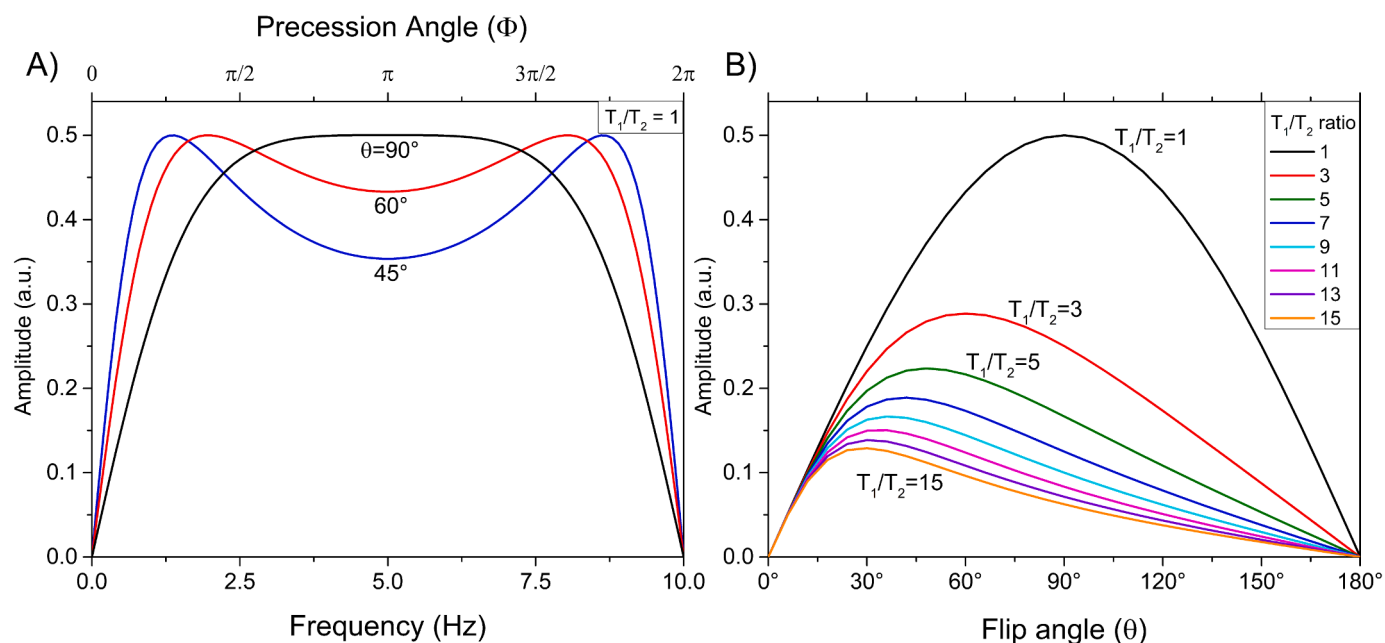**Fig. 4.** Simulations of Eq. (2) of the *Mss* in function of different values of T_1/T_2 ratio, flip angle θ, and precession angle $\Phi = \Omega Tp$, using T_p = 0.1 s. The optimum *Mss* intensity for flip angle θ can be calculated for each situation.

described in the caption of each figure. The temperature of all experiments was 25°C. The codes for the pulse sequences implemented to the TopSpin Bruker spectrometers: SSFPd2, SSFPd4, SSFPd8, and SSFPdxdt, for ^{13}C NMR are in the Supplementary Material.

All spectra acquired by conventional and SSFP pulse sequences were processed by applying an exponential Lorentzian multiplication with a line broadening factor of 1.0 Hz to the FID, followed by Fourier transform (fast Fourier transform algorithm) using a zero-filling factor of 2.

Benchtop SSFP experiments at 1.88 T

Benchtop NMR experiments were performed on a Bruker benchtop Fourier 80 NMR spectrometer, operating at 1.88 T, observing ^{1}H and ^{13}C at 80 and 20 MHz, respectively. The spectrometer is equipped with a 5-mm dual channel (^{1}H and ^{13}C) probe with external lock and actively shielded gradient field. All spectra were acquired at room temperature.

Approximately 35 mg of glucose was dissolved in 0.75 μL D$_2$O. The solution was transferred into 5.0 mm NMR tubes for NMR analysis.

^{13}C{^{1}H} NMR spectra were acquired using standard pulse sequences from the Bruker library, (i.e 30° excitation pulses at 5.6 μs), spectral width (SW) of 240 ppm, recycle delay (D1) of 0.48 s and acquisition time Aq= 0.89 s. The time domain (TD) and NMR signal (FID) were acquired with 8736 datapoints and the sum of 12288 transients, respectively.

^{13}C{^{1}H} NMR SSFPd4 signals were acquired with 30° excitation pulses of 5.6 μs, 4096 transients, SW= 240 ppm, D1= 0.01s, and ranging the Aq of 0.1, 0.2, and 0.49 s. All spectra acquired by conventional and SSFP pulse sequences were processed by applying an exponential Lorentzian multiplication with a line broadening factor of 1.0 Hz to the FID, followed by Fourier transform using a zero-filling factor of 2.

KBDM processing

Krylov basis diagonalization method (KBDM), a parametric method, was used to improve the SSFP spectra resolution, SNR, and to remove the truncation artifacts of conventional Fourier Transform methods. KBDM is a numerical procedure to fit time domain signals as a sum of exponentially damped sinusoids, using Eq. 4.

$$c(t_n) = \sum_{k=0}^{K-1} d_k e^{in\tau\omega_k} \qquad (4)$$

where c(t$_n$) are the data points of the FID, with τ the sampling time interval, $t_n = n\tau$, with n = 0, 1, ..., N-1. The complex amplitudes are $d_k = |d_k|e^{i\theta_k}$, and the complex frequencies $\omega_k = 2\pi f_k + i\gamma_k$, where θ_k are the phases and γ_k the damping constants. The goal of the method is to determine a "line list" of K components of $\{|d_k|, f_k, \theta_k, \gamma_k\}$ that describes all peaks of the spectrum. This line list can eventually be edited to eliminate spurious or unphysical entries, leading to a spectrum more consistent with the input data.

All KBDM processing are based on the same approach of references [16,39,44], using 10k data points for the spectrum. The KBDM algorithm was implemented in C-language in the Code Builder of OriginPro-8.5 (OriginLab Corporation) but, to speed-up the numerical calculations, the necessary mathematical library was separated, optimized, and compiled in professional C or Fortran compilers, generating Dynamic-Link Libraries (DLLs) to be linked with the main program.

Results and discussion

*SSFP experiments in High-Resolution NMR at 14.1 T*

Carbon-13 applications

As suggested by Ernest and Anderson, the pulse interval (T$_p$) must be at least 3T$_2$ to have minimal echo intensity and consequently minimal spectral anomalies. The pulsed NMR experiments are performed with a T$_p$ that is basically the sum of acquisition time (Aq) and recycle delay (D1). For quantitative measurements, common in ^{1}H NMR, the

experiments must be performed with Tp≥ 5T$_1$, to assure that at least 99.33% of the magnetization has returned back to the thermal equilibrium. For nuclei with low receptivity, low gyromagnetic ratio, and low natural abundance, like ^{13}C, normally the NMR spectra are not quantitative (the areas of the signal in the frequency domain are not proportional to the concentration) and T$_p$ is normally much shorter than 5T$_1$, to obtain the maximum SNR.

The conventional ^{13}C NMR pulse sequence proposed by Braun et al. [45] uses a T$_p$ = 1.38 s, composed of Aq and D1 of 0.9 and 0.48 s, respectively. We have demonstrated that with this T$_p$, this sequence is in the SSFP regime as an FID and spin echo signals are observed when Aq~Tp [37]. The default zg30 pulse sequence for the acquisition of ^{13}C NMR spectra in a 14.1 T instrument uses a T$_p$ = 2.9 s, composed of Aq and D1 of 0.9 and 2s, respectively. The default zg30 pulse sequence for the 1.88 T benchtop instrument uses a T$_p$ = 1.24 s, composed of Aq and D1 of 0.84 and 0.2s, respectively.

Considering the T$_2$ of ^{13}C signals for most small molecules, at room temperature, are at least 1s, the default sequence for 14.1 T instruments meets a T$_p$ ≥ 3s, to minimize the echo component. However, the Aq, D1, and T$_p$ used in sequences proposed by Braun et al. [45] or in the default ^{13}C sequences for the benchtop 1.88 T spectrometer are in the SSFP regime. The phase and amplitude anomalies are not observed in the Fourier transformed spectra, using both ^{13}C pulse sequences with T$_p$~T$_2$, because the echo component does not occur during Aq, but during the recycle delay (D1) time. Another reason is that in the ^{13}C NMR experiment, the end of FID signals has low SNR which is minimized by the multiplication of FID by an exponential apodization function that reduces noise and resolution and consequently the echo interference in the Fourier transform spectrum.

Therefore, it is possible to improve the SNR in the ^{13}C spectra (or other low receptivity nuclei) further by reducing the T$_p$ to a much shorter value, using the minimum recycle delay value and a much shorter Aq. However, when the SSFP spectrum is obtained without phase alternation and with short T$_p$~Aq = 0.1s it shows anomalies, as in the ^{13}C spectra of DMSO-d_6 sample that is a septet (Fig. 6A). The septet is distorted in FT spectra (black line) and contains the typical oscillation caused by the truncated FID. Whereas the spectra processed with KBDM (Fig. 6A, red line) does not show the oscillation problem caused by truncated FID, although it shows the amplitude distortion (red line) that
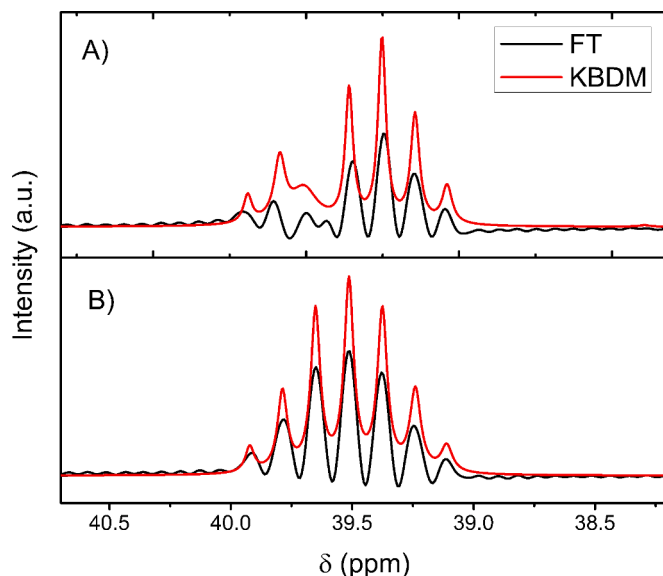
Fig. 6. ^{13}C{^{1}H} NMR spectra of DMSO-d_6 showing the typical septet due to ^{13}C-D spin-spin couplings. The spectra in A were acquired with the SSFP sequence without phase alternation and in B with the SSFPd2 sequence. The Black and red lines are the spectra processed with Fourier Transform and KBDM, respectively.

was caused by the destructive FID/echo interaction.

However, the amplitude anomalies, related to the FID and echo interference cannot always be removed using these parametric methods. Therefore, these FID/echo interferences must be mitigated using pulses sequences that suppress the echo component in the time domain SSFP signal (Fig. 6B).

Fig. 6B shows that phase and amplitude anomalies in the septet of ^{13}C NMR spectrum of DMSO-d_6 sample that has been minimized using the phase alternation pulse sequences (SSFPd2). These sequences suppress the echo component, resulting in a septet without phase and amplitude anomalies and with minimum truncation problem in FT spectrum (black line). As expected, the spectrum processed with KBDM also shows a perfect septet (red line) and no oscillation due to the truncated FID.

Fig. 7 shows an expansion of the ^{13}C NMR spectra of brucine spectra [16] from 80 to 105 ppm, obtained with the SSFPd4 sequence and processed with FT and KBDM. The FT spectrum shows some phase and truncation anomalies that are not observed in the KBDM spectrum. However, the KBDM can introduce some "spurious" signals that may be a problem for its use in structure determination [16].

Fig. 8 shows a comparison of the ^{13}C NMR spectra of sucrose acquired in D_2O obtained with: A) the standard *zgpg30* pulse sequence, with Aq = 0.9 s, D1=2s, 8192 scans, in a total experimental time acquisition of 6h and 46min. Figures B to E show the different SSFP spectra acquired in only 14 min using 8192 scans, with Aq = 0.1s, D1 = 10 ms, and flip angle, θ=90°.

Fig. 8B to E shows the FT spectra acquired with SSFP pulse sequence without phase alternation (B) with two blocks, SSFPd2 (C), with four blocks, SSFPd4 (D), and with eight blocks, SSFPd8 (E). This allowed to more twenty-fold reduction in the acquisition time when compared with conventional zgpg30 pulse sequence (A). Some signals, pointed by the red arrows, acquired with the SSFP sequence without phase alternation (B) are much weaker than the other, indicating a destructive interference of the echo component and phase anomalies.

As expected, these intensity anomalies are reduced using two blocks in the SSFP pulse sequence and minimized by using four and eight blocks. The oscillations observed in all SSFP pulse sequences are due to the FID truncation problem, which can be minimized, using for example Traf [37,38] or trapezoidal apodization functions. They also can be completely suppressed in the spectrum by processing with KBDM or another parametric method [16,39].
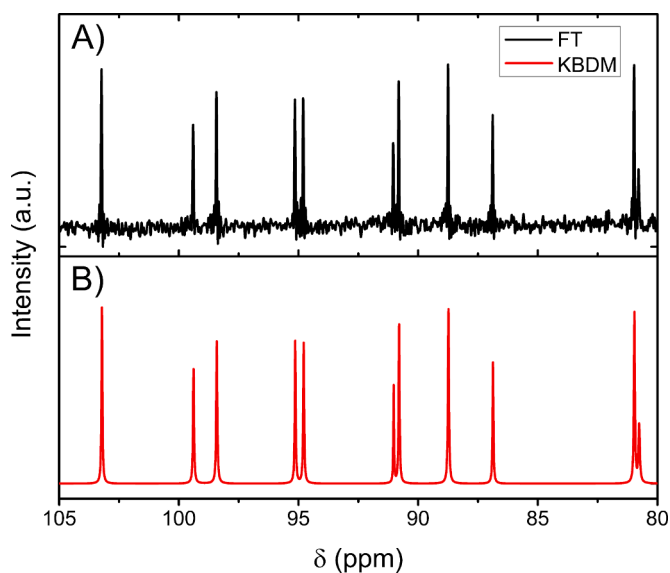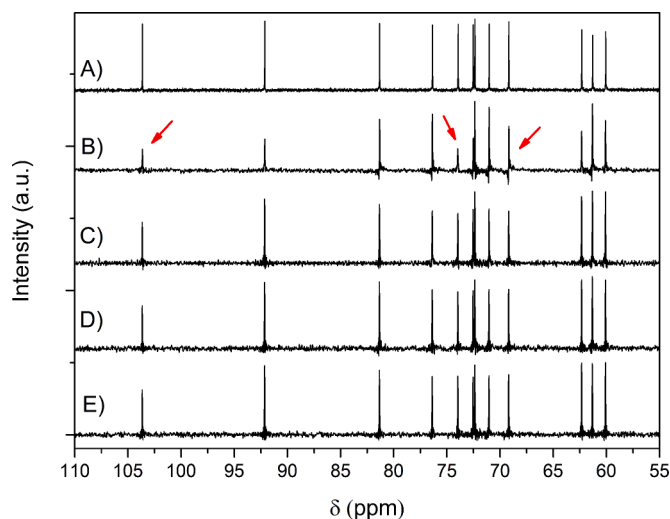

Fig. 8. ^{13}C{^{1}H} NMR spectra of sucrose (D_2O, 14.1 T), obtained with: A) standard zgpg30 pulse sequence, B) SSFP without phase increment, C) SSFPdx with 2 blocks acquisition (SSFPd2), D) SSFPdx with four block acquisition (SSFPd4) and E) SSFPdx with eight block acquisition (SSFPd8). A took 6h and 46 min and B-E took only 14 mins.

It is well known that the integral, in the frequency-domain (i.e., the NMR spectra), or the amplitude, in the time-domain, of ^{13}C NMR signals are not quantitative. This is because the experiments are normally performed without enough time allowing the thermal equilibrium to be reestablished, even when using very small flip angles (e.g., 10°). Similar problems arise by using SSFP pulse sequences, even with phase alternations, because the signal area (frequency-domain) or amplitude (in time-domain) are conditional, not by T_1 but by the T_1/T_2 ratio (Fig. 4B). When $T_1 >> T_2$, Eq. (2) and Fig. 4B shows that the amplitude of the signals acquired with SSFP pulse sequence using 90° excitation pulses is very weak, and in extreme cases, the signals even not observed in the spectrum. Fig. 9 shows the effect of a very large T_1/T_2 ratio for a ^{13}C NMR spectra of ethylbenzene in $CDCl_3$. The chloroform triplet signal at 77 ppm has T_1 = 52 s and T_2 around of 1 s, and it is quite strong in the spectrum acquired with the conventional zgpg30 pulse sequence (Fig. 9A). However, while the spectra were acquired with the SSFPdxdt ($\pi/256$) and SSFPd8 pulse sequences using 90° excitation pulses (Figs. 9B and 9C respectively), the $CDCl_3$ signal is very low, reflecting the large T_1/T_2 ratio. To enhance signal intensities of those nuclides with larger T_1/T_2 ratios, the SSFP spectra can be acquired using optimized low flip angles (Fig. 4B). Fig. 9D to F show the intensity of the $CDCl_3$ signals using SSFPd2 sequences with θ = 30°, 10°, and 5°. Therefore, similar to conventional pulses sequences, amplitude (time-domain) or signal area (frequency-domain) anomalies in ^{13}C spectra can be minimized using low flip angles.

Nitrogen-15 applications

The same idea was used for the acquisition of ^{15}N NMR spectra in natural abundance. Fig. 10 shows the ^{15}N NMR spectra of a mixture of aniline, triethylamine, and deuterated acetonitrile. All the spectra show three signals, around of -350, -340, and -150 ppm which were assigned to triethylamine, aniline, and acetonitrile, respectively. The spectrum acquired with the conventional zg30 sequence (Fig. 10A), demanded 3h and 30 min acquiring while the spectrum acquired with SSFPdxdt ($\pi/256$), Fig. 10B, demanded total time of 30 min. The spectrum obtained with SSFPd4 sequences (not shown) has similar SNR to SSFPdxdt one (Fig. 10B). Both sequences also show similar SNR to the spectrum acquired with standard sequence (Fig. 10A), but in a much shorter time (30 min). These results demonstrate again, the great enhancement in SNR or seven-fold reduction in experimental time achieved when compared with conventional pulse sequences.

Fig. 7. Expanded ^{13}C{^{1}H} NMR spectra of brucine (i.e. 80 to 105 ppm), acquired with SSFPd4 pulse sequence. Black and red lines are the spectra processed with Fourier Transform and KBDM, respectively.
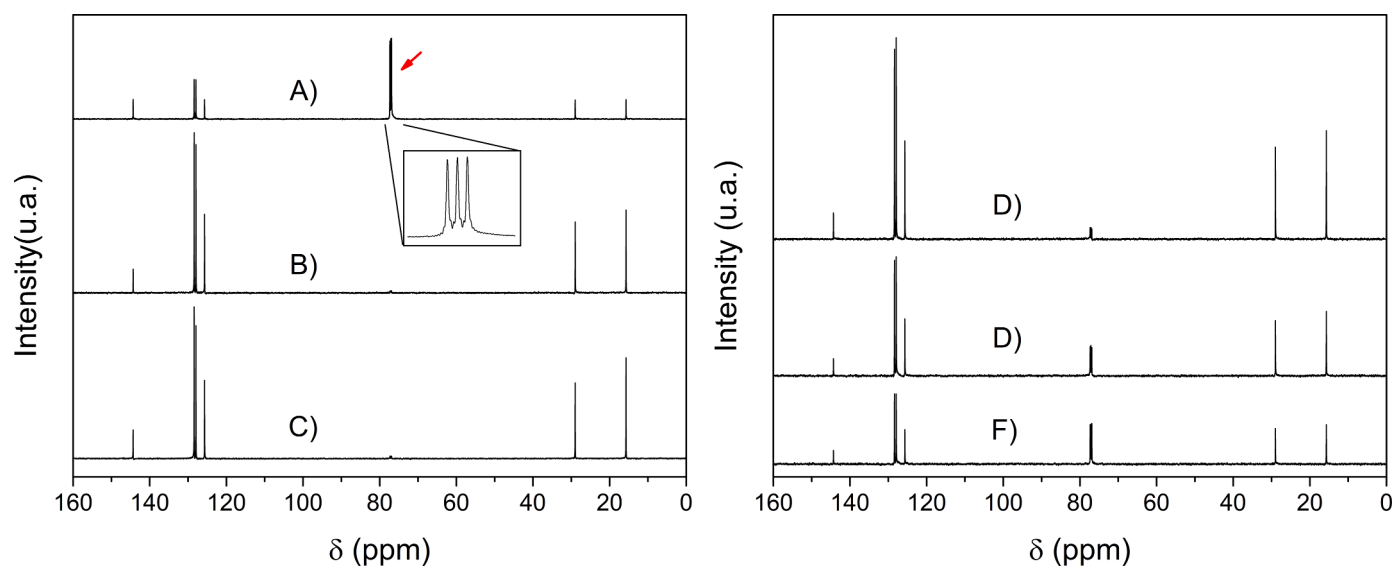
Fig. 9. $^{13}C\{^1H\}$ NMR spectra of ethylbenzene (CDCl$_3$, 14.1 T) acquired with conventional and SSFP pulse sequences. A) Spectrum acquired with the conventional zgpg30 pulse sequence. B and C the spectra were acquired with SSFPdxdt (π/256) and SSFPd8 respectively, both using $\theta = 90°$, Aq = 0.2 s, and 256 scans. The spectra from D to F were obtained with the SSFPdxdt (π/256) sequences with the same parameters of figures B and C, however with $\theta = 30°$, 10°, and 5°, respectively.
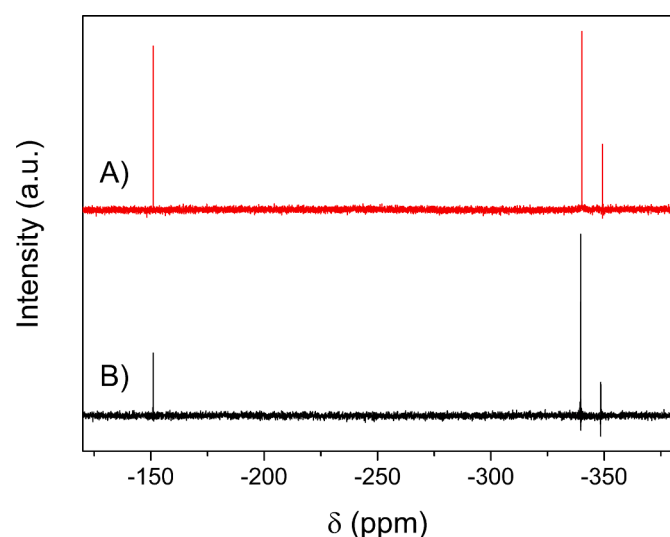
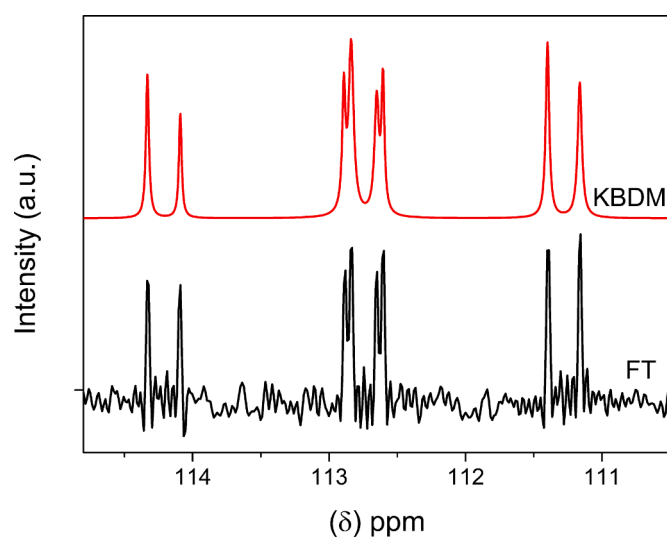**Fig. 10.** Natural abundance $^{15}N\{^1H\}$ spectra of a mixture of 200 µl Aniline, 200 µl of Triethylamine, and 200 µl deuterated acetonitrile. A) Spectrum obtained with the default zg30 sequence acquired in 3h and 30 min and B) spectrum obtained with SSFPdxdt pulse sequence, with π/256, in 30 min.

Fig. 11. ^{15}N NMR spectra of a formamide in natural abundance sample (DMSO-d_6, 14.1 T) acquired with SSFPd2 sequence using $T_p = 400$ ms and processed with FT (black line) and KBDM (red line).

Fig. 11 shows the ^{15}N NMR spectra of formamide, without ^1H decoupling, using SSFPd4 sequence with Aq = 400 ms processed with FT (A) and KBDM method (B). These results show again, the potential of KBDM to obtain a cleaner SSFP spectrum, without the truncation problem.

Phase alternation in the SSFP sequences applied on benchtop NMR spectrometer

As the high and low field Bruker NMR instruments use the same pulse sequences as well as the operation software, the SSFP pulse sequence acquisition parameters are identical, being only necessary to adjust the resonance frequency for each instrument.

The enhancement in SNR in the spectra acquired with SSFP pulse sequences, in low-resolution was demonstrated using a solution of glucose. Fig. 12A shows the $^{13}C\{^1H\}$ NMR spectra acquired with conventional zgpg30 pulse sequence in 4 h, using Aq=0.9, D1=0.48, and

12288 transients [45]. Figs. 12B to D show the spectra acquired with SSFPd4 pulse sequence in 2h, 54 min, and 27 min, using acquisition time of 0.09 s, 0.19 s, and 0.49 s, respectively, D1=0.01s, and 4096 transients. The left and right columns are the spectra processed with FT and KBDM, respectively.

The spectrum acquired with Aq=0.5 s (B) shows much higher SNR in the FT spectrum than the spectrum acquired with zg30 pulse sequences. Furthermore, the spectrum in B also shows similar resolution for the two peaks at approximately 60 and 78 ppm, that those obtained with zg30 sequence, in much longer time. For shorter Aq, the experiments can be performed in much lower experimental time (C and D), however the resolution obtained using FT and KBDM processing are reduced, due to the short Aq.

Conclusion

Challenges and opportunities of SSFP pulse sequences for acquisition
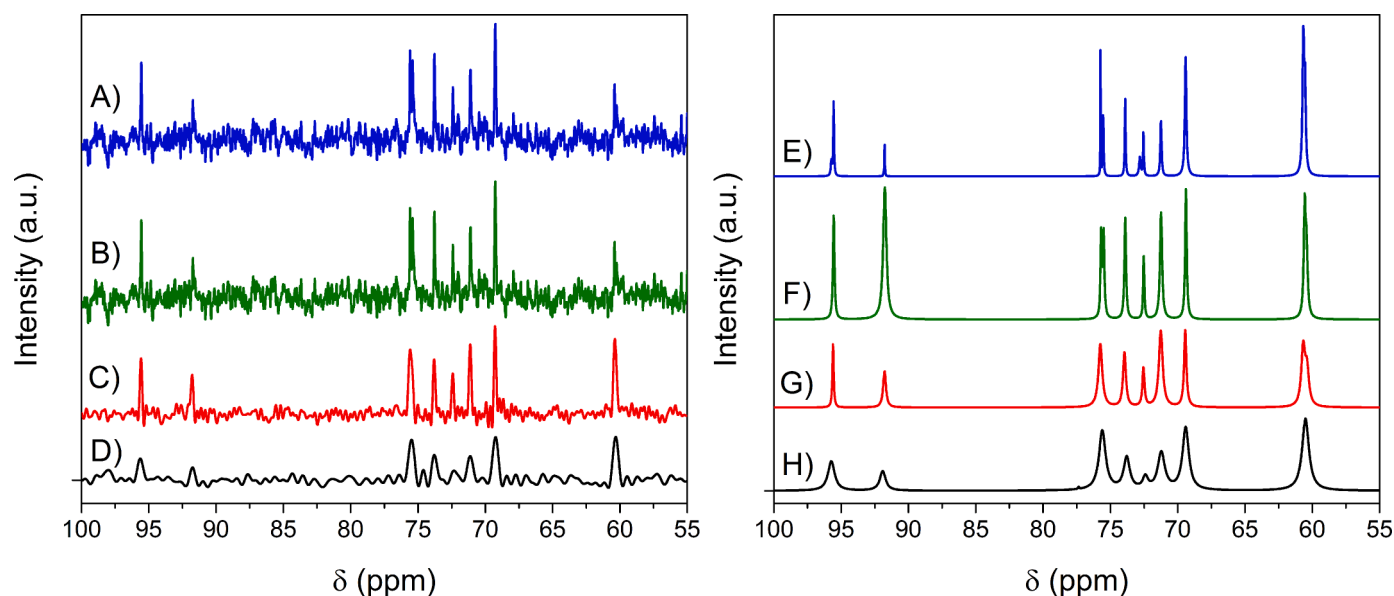
Fig. 12. Medium-resolution SSFPd4 ^{13}C{^{1}H} spectra of glucose acquired with conventional A) zgpg30 and B) to D) SSFPd4 pulse sequences using acquisition time of 0.09 0.19 and 0.49 s, respectively, D1= 0.01 s and 4096 transients, and processed with Fourier Transform E) to H) show the respective spectra, processed using the KBDM method, instead which enables the removal of much of the spectral noise, revealing only the signals of interest.

of NMR spectra in solution samples were presented, as a simple and efficient alternative to enhance SNR, in both high-field and bench-top NMR spectrometers. The gain by using SSFP pulse sequences in acquisition time, in minimum experimental time, is maximum using the shortest time between the pulses, however when Tp<T_2, the constant phase SSFP pulse sequence presents strong phase and amplitude anomalies. In this report, we proposed the use of constant phase increment and a non-constant (or quadratic) phase increment in SSFP pulse sequences to remove the distortions of phase and amplitude observed in conventional SSFP pulse sequence. In addition, the use of KBDM to process NMR spectra, allows to remove sidebands and truncation problems presented in the Fourier Transform spectrum. NMR spectra acquired at low-field (benchtop 1.88 T) and high-field (14.1 T) for ^{1}H, ^{13}C, and ^{15}N nuclei demonstrate the efficiency of these phase alternation in SSFP pulse sequence to remove the phase and amplitude distortions observed in signals obtained by SSFP. The SSFP sequences can also be a viable tool to enhance SNR for those high receptivity nuclei such as ^{19}F and ^{31}P, in very dilute samples, a common scenario in environmental and biological applications.

Declaration of Competing Interest

The authors declare that they have no known competing financial interests or personal relationships that could have appeared to influence the work reported in this paper.

Data availability

Data will be made available on request.

Acknowledgments

Supplementary materials

Supplementary material associated with this article can be found, in the online version, at doi:10.1016/j.jmro.2022.100090.

References

[1] M.H. Levitt, Spin Dynamics: Basics of Nuclear Magnetic Resonance, Wiley, 2001, p. 710.

[2] Bai, S. Nuclear magnetic resonance instrumentation. In Encyclopedia of Analytical Chemistry; pp. 1-26.

[3] T.B. Moraes, L.A. Colnago, Noninvasive analyses of food products using low-field time-domain NMR: a review of relaxometry methods, Brazilian J. Phys. 52 (2022), https://doi.org/10.1007/s13538-022-01055-1.

[4] B. Blumich, Introduction to compact NMR: a review of methods, Trac-Trends in Analytical Chem. 83 (2016) 2–11, https://doi.org/10.1016/j.trac.2015.12.012.

[5] J.H. Ardenkjaer-Larsen, G.S. Boebinger, A. Comment, S. Duckett, A.S. Edison, F. Engelke, C. Griesinger, R.G. Griffin, C. Hilty, H. Maeda, et al., Facing and overcoming sensitivity challenges in biomolecular NMR spectroscopy, Angewandte Chemie-Int. Edition 54 (2015) 9162–9185, https://doi.org/10.1002/anie.201410653.

[6] Z.F. Wang, Y.L. You, F.F. Li, W.R. Kong, S.Q. Wang, Research progress of NMR in natural product quantification, Molecules 26 (2021), https://doi.org/10.3390/molecules26206308.

[7] Q.X. Gong, A. Gordji-Nejad, B. Blumich, S. Appelt, Trace analysis by low-field NMR: breaking the sensitivity limit, Analytical Chem. 82 (2010) 7078–7082, https://doi.org/10.1021/ac101738f.

[8] R.E. Mewis, K.D. Atkinson, M.J. Cowley, S.B. Duckett, G.G.R. Green, R.A. Green, L. A.R. Highton, D. Kilgour, L.S. Lloyd, J.A.B. Lohman, et al., Probing signal amplification by reversible exchange using an NMR flow system, Magnetic Resonance in Chem. 52 (2014) 358–369, https://doi.org/10.1002/mrc.4073.

[9] A.J. Simpson, M.J. Simpson, R. Soong, Environmental nuclear magnetic resonance spectroscopy: an overview and a primer, Analytical Chem. 90 (2018) 628–639, https://doi.org/10.1021/acs.analchem.7b03241.

[10] P.C.A. van der Wel, K.N. Hu, J. Lewandowski, R.G. Griffin, Dynamic nuclear polarization of amyloidogenic peptide nanocrystals: GNNQQNY, a core segment of the yeast prion protein Sup35p, J. Am. Chem. Soc. 128 (2006) 10840–10846, https://doi.org/10.1021/ja0626685.

[11] N. Eshuis, B.J.A. van Weerdenburg, M.C. Feiters, F. Rutjes, S.S. Wijmenga, M. Tessari, Quantitative Trace Analysis of Complex Mixtures Using SABRE

Hyperpolarization, Angewandte Chemie-Int. Edition 54 (2015) 1481–1484, https://doi.org/10.1002/anie.201409795.

[12] N.K. Bangerter, B.A. Hargreaves, S.S. Vasanawala, J.M. Pauly, G.E. Gold, D.G. Nishimura, Analysis of multiple-acquisition SSFP, Magnetic Resonance in Medicine 51 (2004) 1038–1047, https://doi.org/10.1002/mrm.20052.

[13] O. Speck, K. Scheffler, J. Hennig, Fast 31P chemical shift imaging using SSFP methods, Magnetic Resonance in Med. 48 (2002) 633–639.

[14] R.B.D. Azeredo, M. Engelsberg, L.A. Colnago, Flow sensitivity and coherence in steady-state free spin precession, Phys. Rev. E 64 (2001) 4, https://doi.org/10.1103/PhysRevE.64.016309.

[15] R.B.V. Azeredo, L.A. Colnago, A.A. Souza, M. Engelsberg, Continuous wave free precession - practical analytical tool for low-resolution nuclear magnetic resonance measurements, Analytica Chimica Acta 478 (2003) 313–320, https://doi.org/10.1016/s0003-2670(02)01514-3.

[16] T.B. Moraes, P.M. Santos, C.J. Magon, L.A. Colnago, Suppression of spectral anomalies in SSFP-NMR signal by the Krylov basis diagonalization method, J. Magnetic Resonance 243 (2014) 74–80, https://doi.org/10.1016/j.jmr.2014.03.009.

[17] T. Wolf, M.J. Jaroszewicz, L. Frydman, Steady-state free precession and solid-state NMR: how, when, and why, J. Phys. Chem. C 125 (2021) 1544–1556, https://doi.org/10.1021/acs.jpcc.0c09696.

[18] R. Bradford, C. Clay, E. Strick, A steady-state transient technique in nuclear induction, Phys. Rev. 84 (1951) 157–158, https://doi.org/10.1103/PhysRev.84.157.

[19] H.Y. Carr, Steady-state free precession in nuclear magnetic resonance, Phys. Rev. 112 (1958) 1693–1701, https://doi.org/10.1103/PhysRev.112.1693.

[20] T.B. Moraes, T. Monaretto, L.A. Colnago, Rapid and simple determination of T-1 relaxation times in time-domain NMR by continuous wave free precession sequence, J. Magnetic Resonance 270 (2016) 1–6, https://doi.org/10.1016/j.jmr.2016.06.019.

[21] J. Kronenbitter, A. Schwenk, New technique for measuring relaxation-times T1 and T2 and equilibrium magnetization M0 of slowly relaxing systems with weak NMR signals, J. Magnetic Resonance 25 (1977) 147–165, https://doi.org/10.1016/0022-2364(77)90127-5.

[22] T.B. Moraes, Precessão Livre no Estado Estacionário com alternância de fase para RMN em alta e baixa resolução, Tese (Doutorado em Física), Instituto de Física de São Carlos, Universidade de São Paulo, (USP), (2016) 172, https://doi.org/10.11606/T.76.2016.tde-14102016-091634.

[23] R.R. Ernst, W.A. Anderson, Application of Fourier Transform spectroscopy to magnetic resonance, Rev. Sci. Instruments 37 (1966) 93, https://doi.org/10.1063/1.1719961. -+.

[24] T. Monaretto, F.D. Andrade, T.B. Moraes, A.A. Souza, E.R. deAzevedo, L.A. Colnago, On resonance phase alternated CWFP sequences for rapid and simultaneous measurement of relaxation times, J. Magnetic Resonance 259 (2015) 174–178, https://doi.org/10.1016/j.jmr.2015.08.013.

[25] T. Monaretto, E.T. Montrazi, T.B. Moraes, A.A. Souza, C. Rondeau-Mouro, L.A. Colnago, Using T-1 as a direct detection dimension in two-dimensional time-domain NMR experiments using CWFP regime, J. Magnetic Resonance 311 (2020), https://doi.org/10.1016/j.jmr.2019.106666.

[26] T.B. Moraes, T. Monaretto, L.A. Colnago, Applications of continuous wave free precession sequences in low-field, time-domain NMR, Appl. Sci.-Basel 9 (2019), https://doi.org/10.3390/app9071312.

[27] A. Schwenk, NMR pulse technique with high sensitivity for slowly relaxing systems, J. Magnetic Resonance 5 (1971) 376, https://doi.org/10.1016/0022-2364(71)90088-6. -&.

[28] J. Kronenbitter, A. Schwenk, New technique for measuring relaxation-times T1 and T2 and equilibrium magnetization M0 of slowly relaxing systems with weak NMR

[29] signals, J. Magnetic Resonance 25 (1977) 147–165, https://doi.org/10.1016/0022-2364(77)90127-5.

[29] R.B.D. Azeredo, L.A. Colnago, M. Engelsberg, Quantitative analysis using steady-state free precession nuclear magnetic resonance, Analytical Chem 72 (2000) 2401–2405, https://doi.org/10.1021/ac991258e.

[30] L.A. Colnago, R.B.V. Azeredo, A.M. Netto, F.D. Andrade, T. Venancio, Rapid analyses of oil and fat content in agri-food products using continuous wave free precession time domain NMR, Magnetic Resonance in Chem. 49 (2011) S113–S120, https://doi.org/10.1002/mrc.2841.

[31] T. Venancio, L.A. Colnago, Simultaneous measurements of T1 and T2 during fast polymerization reaction using continuous wave-free precession NMR method, Magnetic Resonance in Chem. 50 (2012) 534–538, https://doi.org/10.1002/mrc.3834.

[32] M.G.A. Carosio, D.F. Bernardes, A.D. Carvalho, L.A. Colnago, Non-invasive measurements of oilseed temperature in soil and soil thermal diffusivity using time-domain NMR relaxometry, Appl. Magnetic Resonance 49 (2018) 1119–1127, https://doi.org/10.1007/s00723-018-1028-8.

[33] E.T. Montrazi, T. Monaretto, T.J. Bonagamba, L.A. Colnago, New and rapid pulse sequences for two-dimensional D-T-1 correlation measurements, J. Magnetic Resonance (2020) 315, https://doi.org/10.1016/j.jmr.2020.106749.

[34] T. Monaretto, T.B. Moraes, L.A. Colnago, Recent 1D and 2D TD-NMR pulse sequences for plant science, Plants-Basel 10 (2021), https://doi.org/10.3390/plants10050833.

[35] C.J. Duarte, L.A. Colnago, R.B.D. Azeredo, T. Venancio, Solvent suppression in high-resolution H-1 NMR spectroscopy using conventional and phase alternated continuous wave free precession, Appl. Magnetic Resonance 44 (2013) 1265–1280, https://doi.org/10.1007/s00723-013-0482-6.

[36] R. Freeman, H.D.W. Hill, Phase and intensity anomalies in fourier transform NMR, J. Magnetic Resonance 4 (1971) 366, https://doi.org/10.1016/0022-2364(71)90047-3. -&.

[37] P.M. dos Santos, A.A. de Souza, L.A. Colnago, Fast acquisition of C-13 NMR spectra using the steady-state free precession sequence, Appl. Magnetic Resonance 40 (2011) 331–338, https://doi.org/10.1007/s00723-011-0209-5.

[38] D.D. Traficante, G.A. Nemeth, A New and improved apodization function for resolution enhancement in NMR-spectroscopy, J. Magnetic Resonance 71 (1987) 237–245, https://doi.org/10.1016/0022-2364(87)90053-9.

[39] L.M.S. Nunes, T.B. Moraes, L.L. Barbosa, L.H. Mazo, L.A. Colnago, Monitoring electrochemical reactions in situ using steady-state free precession 13C NMR spectroscopy, Analytica Chimica Acta 850 (2014) 1–5, https://doi.org/10.1016/j.aca.2014.05.022.

[40] K.S. Nayak, H.L. Lee, B.A. Hargreaves, B.S. Hu, SSFP Wideband, Alternating repetition time balanced steady state free precession with increased band spacing, Magnetic Resonance in Med. 58 (2007) 931–938, https://doi.org/10.1002/mrm.21296.

[41] K.L. Miller, FMRI using balanced steady-state free precession (SSFP), Neuroimage 62 (2012) 713–719, https://doi.org/10.1016/j.neuroimage.2011.10.040.

[42] T.N. Rudakov, Modification of SSFP technique for the effective detection of NQR signals, Phy. Lett. A 358 (2006) 322–326, https://doi.org/10.1016/j.physleta.2006.05.024.

[43] T.N. Rudakov, Some aspects of the effective detection of ammonium nitrate-based explosives by pulsed NQR method, Appl. Magnetic Resonance 43 (2012) 557–566, https://doi.org/10.1007/s00723-012-0330-0.

[44] R.M. Maria, T.B. Moraes, C.J. Magon, T. Venancio, W.F. Altei, A.D. Andricopulo, L.A. Colnago, Processing of high resolution magic angle spinning spectra of breast cancer cells by the filter diagonalization method, Analyst 137 (2012) 4546–4551, https://doi.org/10.1039/c2an35451a.

[45] N. Mills, 150 and more basic NMR experiments: a practical course, 2nd edition (Braun, S.; Kalinowski, H.-O.; Berger, S.), J. Chemical Education 77 (2000) 831.